# Micromagnetic Models of the Effect of Particle Shape on Magnetic Hysteresis

*Yongjae Yu*
*Department of Geology and Earth Environmental Sciences, Chungnam National University, Daejeon, 305-764, Korea.*
*Lisa Tauxe*
*Geosciences Research Division, Scripps Institution of Oceanography, La Jolla, CA 92093-0220, USA.*

**Abstract**

Direct calibration of magnetic hysteresis with grain size is of particular interest for sub-micron particles. In the present study, we numerically tested the effect of particle shape (grain morphology and aspect ratio) on magnetic hysteresis of stress-free $Fe_3O_4$. We found that the particle shape has a profound effect on hysteresis behavior. In particular, for particles with grain width > 120 nm, octahedra (and tetragonally terminated prisms) showed higher coercivity and squareness than cubes (and rectangular parallelepipeds) due to an inherent geometric advantage. Results from micromagnetic calculations and experimental observations are somewhat mismatching. It is likely that stress-free $Fe_3O_4$ used in hysteresis experiments were not entirely stress-free or the grain size of stress-free $Fe_3O_4$ was overestimated on using two-dimensional images of three-dimensional objects.

## 1. Introduction

Micromagnetic modeling (Brown, 1963) explores magnetic configurations in nano-scales as well as the magnetic reversal process in magnetic systems. Micromagnetic models visualize the details of magnetic domain structures, and also can produce snapshots of complex remanence or other magnetic states. Unlike classical domain theories with a discrete number of domains (e.g., Kittel, 1949), modern micromagnetic calculations reveal non-uniform magnetization structures such as flower or vortex states (Schabes and Bertram, 1988; Williams and Dunlop, 1989). The most eye-catching discovery was the evolution of non-uniform magnetization states from the uniform magnetization state in single-domain (SD) to distinct domain walls in multidomain (MD) (Schabes and Bertram, 1988, Williams and Dunlop, 1989). Since these initial developments, there has been noticeable progress in modeling $Fe_3O_4$ (e.g., Williams and Dunlop, 1990; Newell et al., 1993a, 1993b; Williams and Dunlop, 1995; Fabian et al., 1996; Xu and Dunlop, 1996; Fukuma and Dunlop, 1997, 1998, 2006; Winklehofer et al., 1997; Williams and Wright, 1998; Rave et al., 1998; Muxworthy and Williams, 1999a, 1999b; Newell and Merrill, 1999, 2000; Tauxe et al., 2002; Muxworthy et al., 2003a, 2003b; Witt et al., 2005; Yu and Tauxe, 2005; Carvallo et al., 2006; Williams et al., 2006).

Magnetic hysteresis originates from a sequence of irreversible flipping of particle moments by exposure to changes in magnetic fields. The field at which particle flipping occurs is known as the "switching field", and is controlled by many factors such as composition, grain shape and size, prior field treatment, and stress effects (e.g., Yu et al., 2004). Among various factors that govern magnetic properties in a magnetic system, grain geometry (crystal morphology) has seldom been highlighted in micromagnetism. In fact, a common approach in modeling magnetic hysteresis of $Fe_3O_4$ has been to model cubic or rectangular parallelepiped grains of $Fe_3O_4$ (e.g., Yu and Tauxe, 2005). However, synthetically produced $Fe_3O_4$ shows a wide spectrum of morphology. For instance, qua si-spherical forms exist for synthetic $Fe_3O_4$ that are produced from aqueous solution (Amin et al., 1987; Heider et al., 1987). In addition, biogenic $Fe_3O_4$ in magnetotactic bacteria typically show octahedral or octahedral prismatic structures, although cubo-octahedral morphology has been documented as well (Frankel et al., 1998).

Although largely ignored, the effect of grain morphology has been previously studied to some extent. While the effect of irregular shapes or grain elongations were briefly considered in the past (e.g., Williams and Dunlop, 1990; Fabian et al., 1996; Fabian and Hubert, 1999), Williams and Wright (1998) first introduced the grain geometry effect systematically in modeling $Fe_3O_4$. They observed that flower-vortex transition occurred at lower grain volumes for octahedron than for cube. Witt et al. (2005) recently reported that flower states can persist up to much larger grain sizes in octahedral morphologies than in cubes, providing a plausible answer for an anomalously high ratio of TRM/ARM (thermoremanent magnetization over anhysteretic remanent magnetization) observed in stress-free submicron $Fe_3O_4$ (e.g., Dunlop and Argyle, 1997; Yu et al., 2003). Recently, Williams et al. (2006) showed that the coercivity and critical single-domain boundary of $Fe_3O_4$ is strongly dependent on the type of dominant magnetic anisotropy and particle morphology. In the present study, we plan to incorporate the effect of grain morphology and aspect ratio on micromagnetic hysteresis simulation.

The present study was intended (1) to model the magnetic hysteresis for the cubic- and octahedron geometry of $Fe_3O_4$ with various grain elongations and (2) to compare model predictions with the previously documented experimental observations of stress-free $Fe_3O_4$.

## 2. Micromagnetic modeling

The program and methodology used in the present study were fully described elsewhere (Seberino and Bertram, 2001; Tauxe et al., 2002; Yu and Tauxe, 2005), hence only a brief summary is given here. The total free energy in a given magnetic system is a summation of the exchange energy, magnetic potential energy, magnetocrystalline energy, magnetoelastic energy, and magnetostatic energy. The magnetic spin configuration in a given system is determined by minimizing the total free energy.

In cubic modeling (e.g., Bertram and Zhu, 1992), we discretized particles into cubic elements with cell dimension *s* within which the magnetization is uniform (Figure 1a). We used a Fast Multipole Code (FMM) (see Seberino and Bertram, 2001) that integrates the coupled Landau-Lifshitz-Gilbert equation. Our approach included magnetocrystalline anisotropy and attempts to incorporate the effect of grain size, particle shape, and orientation of the external field. In the present study, the effect of magnetostriction and thermal fluctuations are not counted because we are interested only in stress-free $Fe_3O_4$. We simulated $Fe_3O_4$ particles that range from 40 to 200 nm.

**Fig.1**

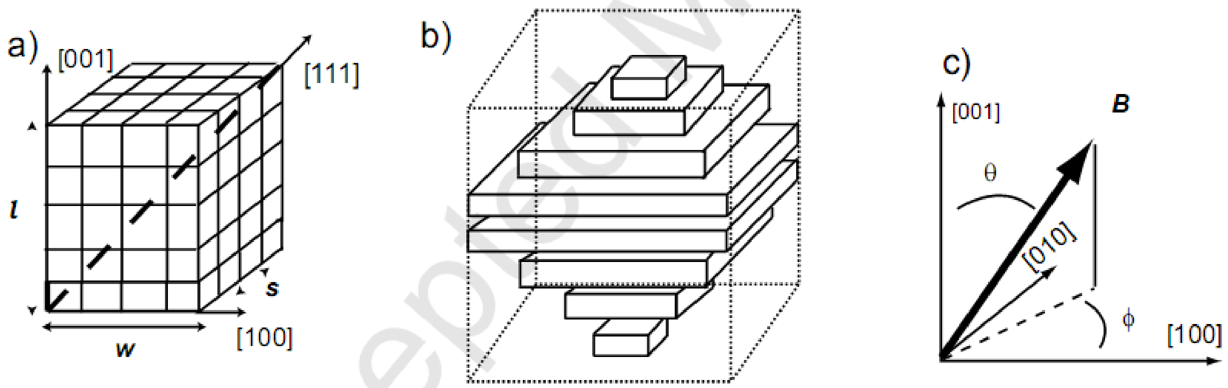


In the present study, we have extended the analysis to include octahedral shapes. This was done by masking out selected elements in the cube (Figure 1b). For example, the 6x6x6 cubic equivalent octahedron contains 6 layers of arrays of 2x2, 4x4, 6x6, 6x6, 4x4, and 2x2 (see a schematic drawing in Figure 1b; see also Williams and Wright (1998)). In octahedral simulations, we maintained an even number of arrays for each vertical layer to minimize the stray field effects. We set particle elongation along the [001] direction for convenience. Elongation for the octahedra was achieved by adding an appropriate number of the widest layers in the middle of the vertical sections. For example, to simulate an aspect ratio *(q* = major axis / minor axis) of *q=1.5* in Figure 1b, we used 9 layers of arrays of 2x2, 4x4, 6x6, 6x6, 6x6, 6x6, 6x6,4x4, and 2x2.

Strictly speaking, we used a tetragonally terminated prism instead of an elongated octahedron to better control the robustness of the solution and to minimize the stray field effects. Such inherent limitation results from the fact that the modeled meshes are built on cube elements. It would be interesting to compare our results with those for Williams et al. (2006) who used finite element approach with tetrahedral elements. To reasonably model microstructures, an element size needs to be regulated. The exchange length of $Fe_3O_4$ is 9.6 nm (Rave et al., 1998). In the present study, varying element size of 8-10 nm was used. The relationship of the applied field B to the three major crystallographic axes is expressed as $\theta$ and $\phi$ (Figure 1c).

For each configuration, we simulated one full hysteresis loop by cycling through from positive to negative saturation, then back to positive saturation magnetization state. To detect and avoid the possible instability of our numerical solutions, we repeated all simulations with different field increments/decrements of 1 and 0.5 mT. Whenever we found dual solutions, we use the smoother (with less drastic jumps) hysteresis behavior as the ultimate solution. The material constants, chosen for room temperature T = 298 K, wereA = $1.32 \times 10^{-11}$ J/m, $M_s = 4.80 \times 10^5$ A/m, andK1 = $-1.25 \times 10^4$ J/m$^3$.

To represent magnetic hysteresis produced by a set of randomly oriented magnetic grains, we need to carry out hysteresis simulations along many different directions because magnetic hysteresis is inherently dependent on the direction of initial magnetic saturation. We therefore calculated magnetic hysteresis along 18 different directions that are more or less equally distributed in a three-dimensional space; [45, 1], [1, 45] [15, 45], [30, 45], [45, 45], [55, 45], [60, 45], [75, 45], [89, 45], [45, 54.7], [1, 89], [15, 89], [30, 89], [45, 89], [55, 89], [60, 89], [75, 89], [89, 89] in terms of $\phi$ and $\theta$. Note that [$\phi$ = 45, $\theta$ = 54.7] represents the magnetic easy axes of $Fe_3O_4$. Averages of these 18 simulations were used as to represent magnetic hysteresis for an ensemble of randomly oriented $Fe_3O_4$.

**3. Snapshots of Micromagnetic Calculation**

To visualize the grain geometry effect, we present snapshots of magnetic configuration at the remanence state for representative simulations (Figures 2-4). Observations of snapshots for simulations can be categorized into three types. First, grain widths in the range of 40-80 nm always showed quite uniform magnetization configurations with a dominant flower remanent state (e.g., Figure 2). For instance, the magnetic configuration of saturation remanent magnetization for 80 nm grains of *q=1.5* along the [111] direction revealed typical flower structures with fairly high squareness (= saturation remanence $M_r$ / saturation magnetization $M_s$) of 0.44 for rectangular parallelepiped and 0.39 for tetragonally terminated prism, respectively (Figure 2). For 40-80 nm widths, we observed a flower state regardless of the applied field direction, aspect ratio, or grain geometry.

**Fig.2**

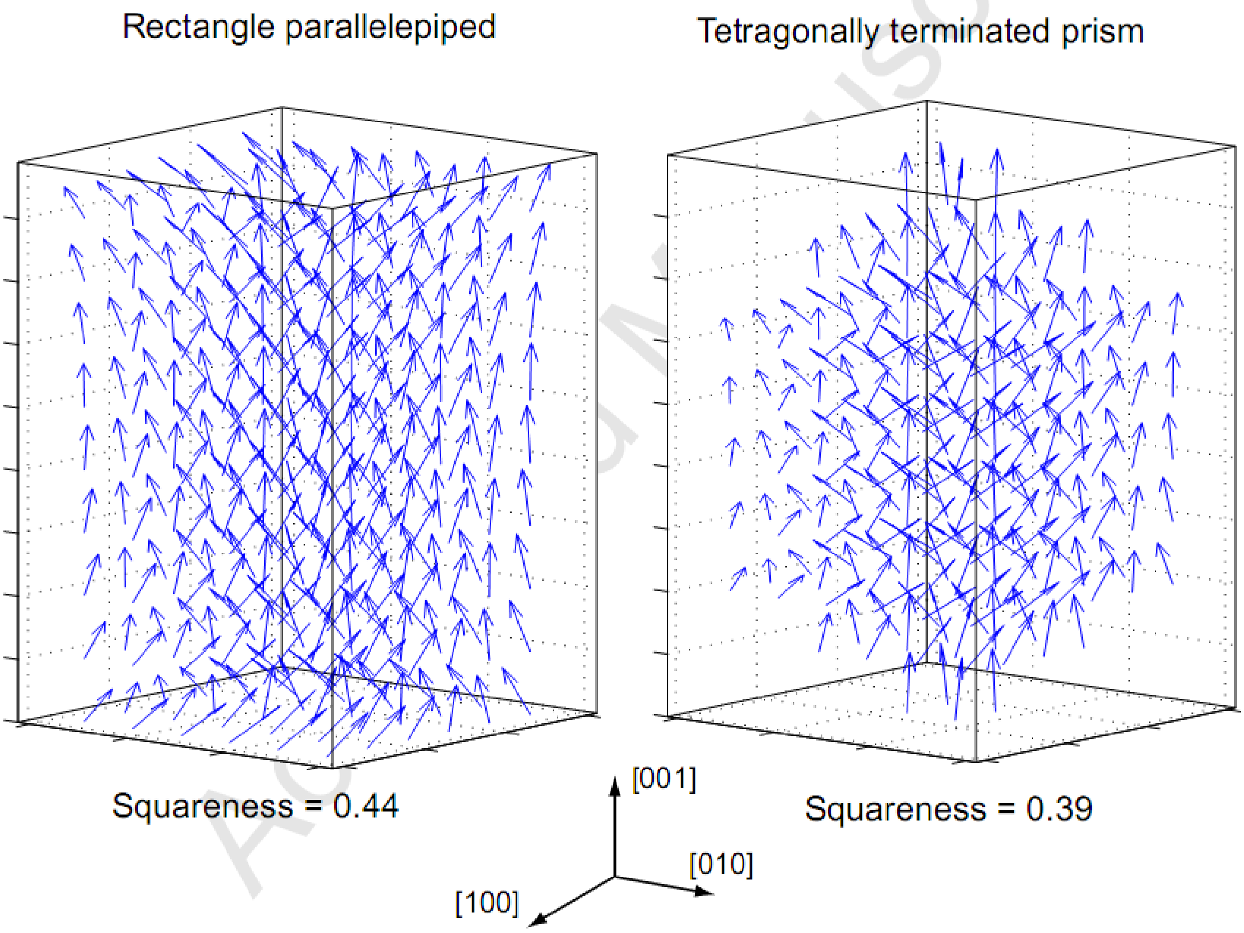


Second, grain widths in the 90-160 nm range showed a dominant vortex remanent state with squareness of 0.1-0.2 (e.g., Figure 3). For 140 nm $Fe_3O_4$ of q=1.25, snapshots illustrated quite different vortex structures dependent on the particle morphology. The magnetic structure of the octahedron had a consistent vorticity (sense of rotation with respect to the center) while that of the parallelepiped changed direction from top to bottom (Figure 3). Third, grain widths in > 160 nm usually recorded near-zero remanence for cuboids but some remanence for octahedra (e.g., Figure 4). For 200 nm cubic $Fe_3O_4$, we found a vortex remanent state with near-zero remanence (Figure 4; left panel). On the other hand, the equivalent octahedral $Fe_3O_4$ preserved a squareness of 0.08, aligning magnetic spins along [001] for the central 4 columns (Figure 4; right panel).

**Fig.3**

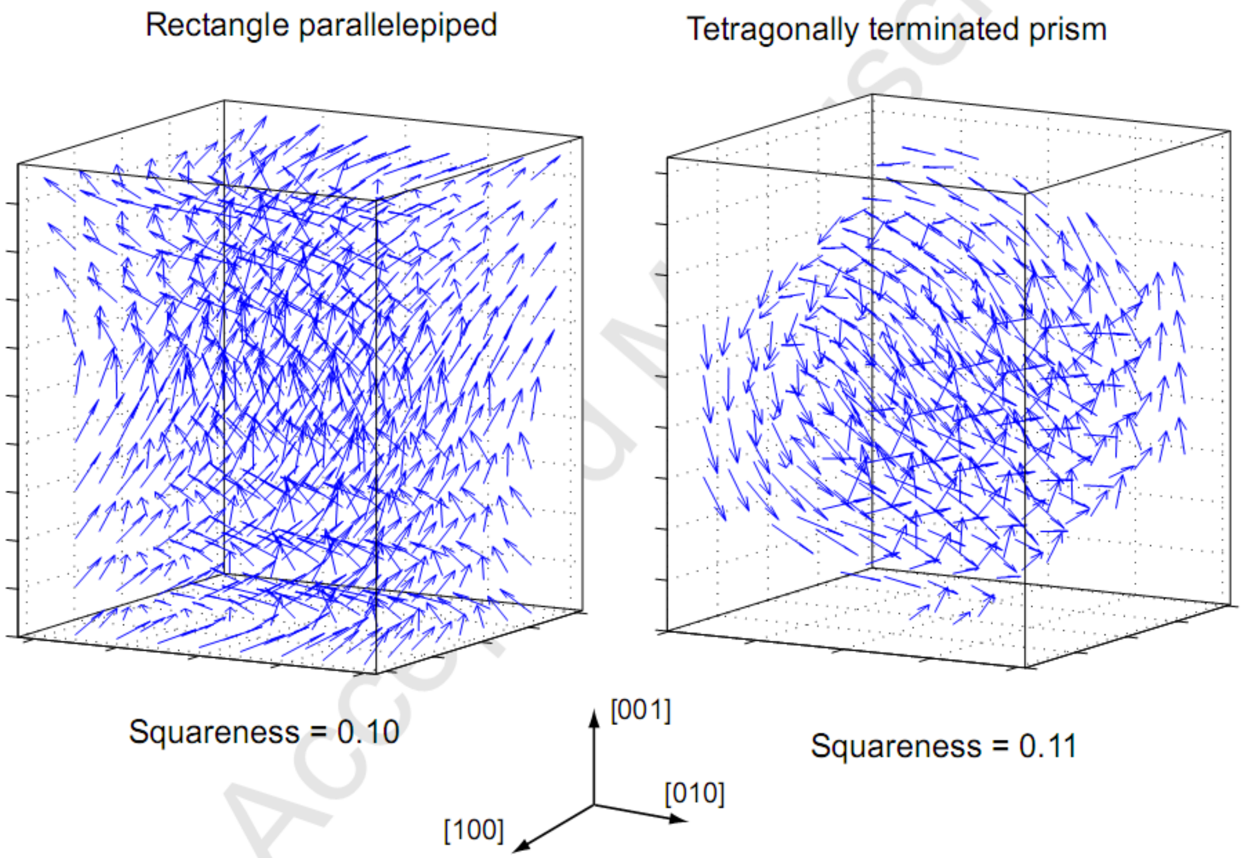


**Fig.4**

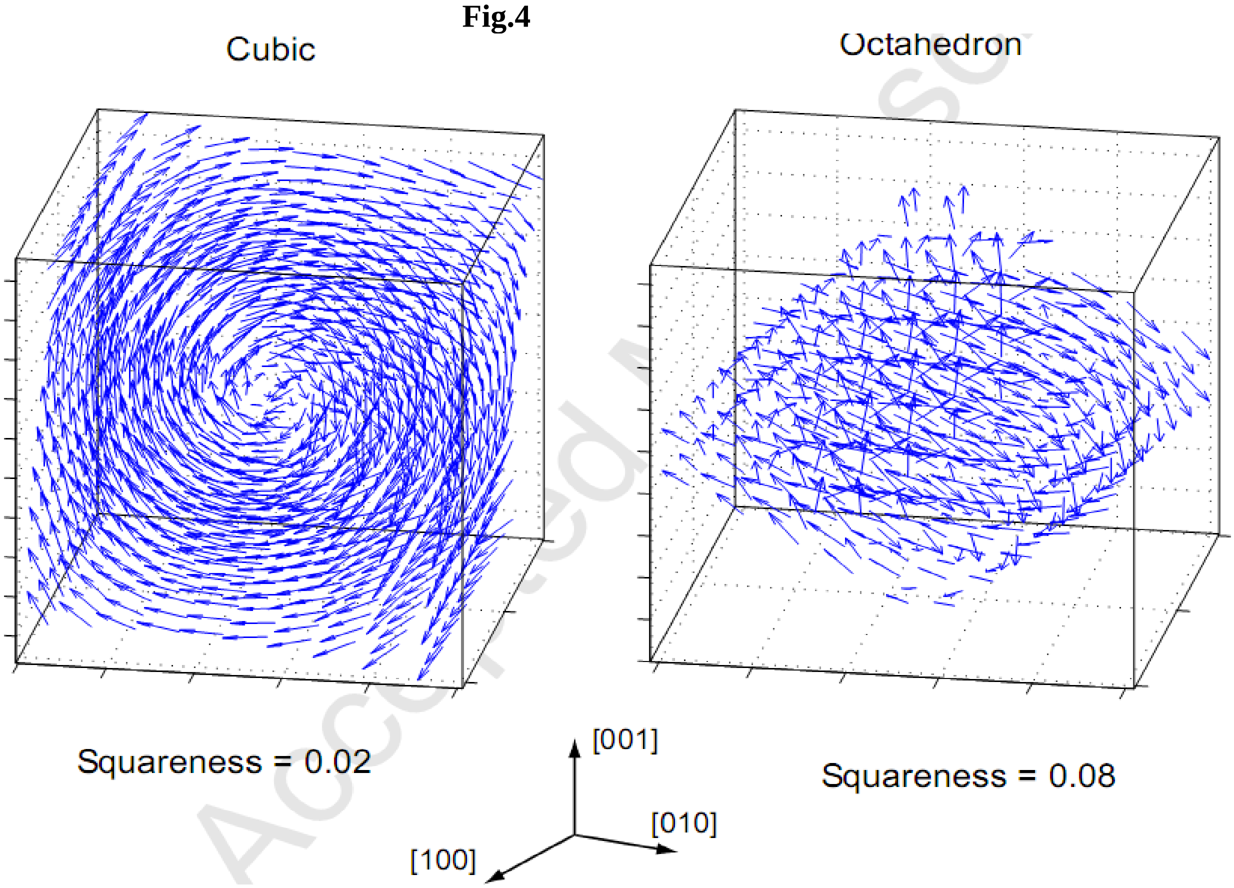

## 4. Properties of Magnetic Hysteresis

*4-1. Single-domain and Vortex Transition*

Grain widths in 40-80 nm showed a prevalence of flower structures. For equant $Fe_3O_4$, grain widths in 40-80 nm displayed squareness > 0.80, fairly close to the ideal squareness of cubic single-domain (CSD) (=0.866) (Figure 5). Of course, smaller grains (e.g., 40 nm widths) marked slightly higher squareness than the larger one (e.g., 80 nm width) due to more concentrated (and much more uniform) flower structures. As the aspect ratio increased, squareness for 40-80 nm $Fe_3O_4$ converged towards the uniaxial single-domain (USD) value of 0.5 (Figure 5).

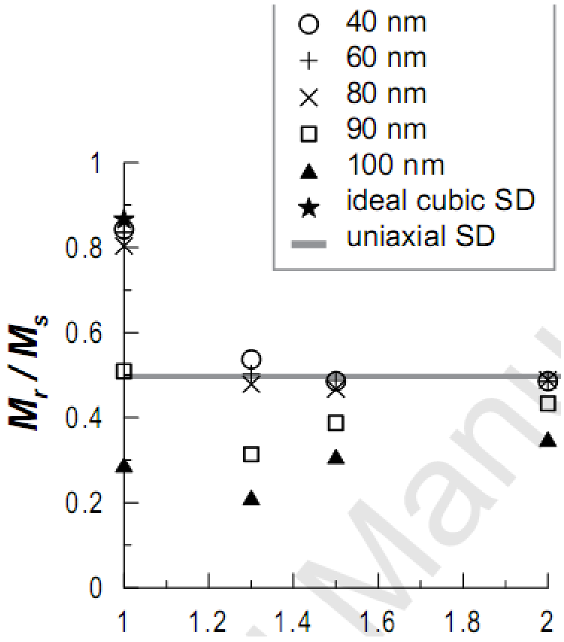


Grain widths > 80 nm showed different aspects with squareness far less than CSD (for equant particle) and USD (for elongated particle). It is apparent that a flower-vortex transition occurred at 80-90 nm, by implication SD - pseudo-single-domain (PSD) boundary (Figure 5). It is important that notable changes in squareness is evident at 80-90 nm whether the grain is elongated or not (Figure 5). For equant particles, it has been documented that the SD-PSD boundary lies at 60-70 nm (e.g., Newell et al., 1993; Fabian et al., 1996; Williams and Wright, 1998; Muxworthy et al., 2003b; Fukuma and Dunlop, 2006), although larger transition values of 80-90 nm were also reported (e.g., Witt et al., 2005).

Comparing our results with other modeling data provides the minimum quality-control. In the literature, great wealth of squareness data is available for the equant cubes. However, magnetic hysteresis is strongly dependent on the direction of applied field, thus the results must be compared under the same orienting condition. For magnetic hysteresis along the magnetocrystalline axis [111], our data and three other previous results displayed similar variations. However, each result showed different SD-PSD transition volume. For instance, drastic drop of squareness along [111] (e.g., SD-PSD transition) was recorded in 60-70 nm (Williams et al., 2006), in 70-80 nm (Fukuma and Dunlop, 2006), in 80-90 nm (this study), and much larger (Fabian et al., 1996). Such a gap persists even when the random assembly of $Fe_3O_4$ grain is taken into account (see solid circles versus solid squares in Figure 6).

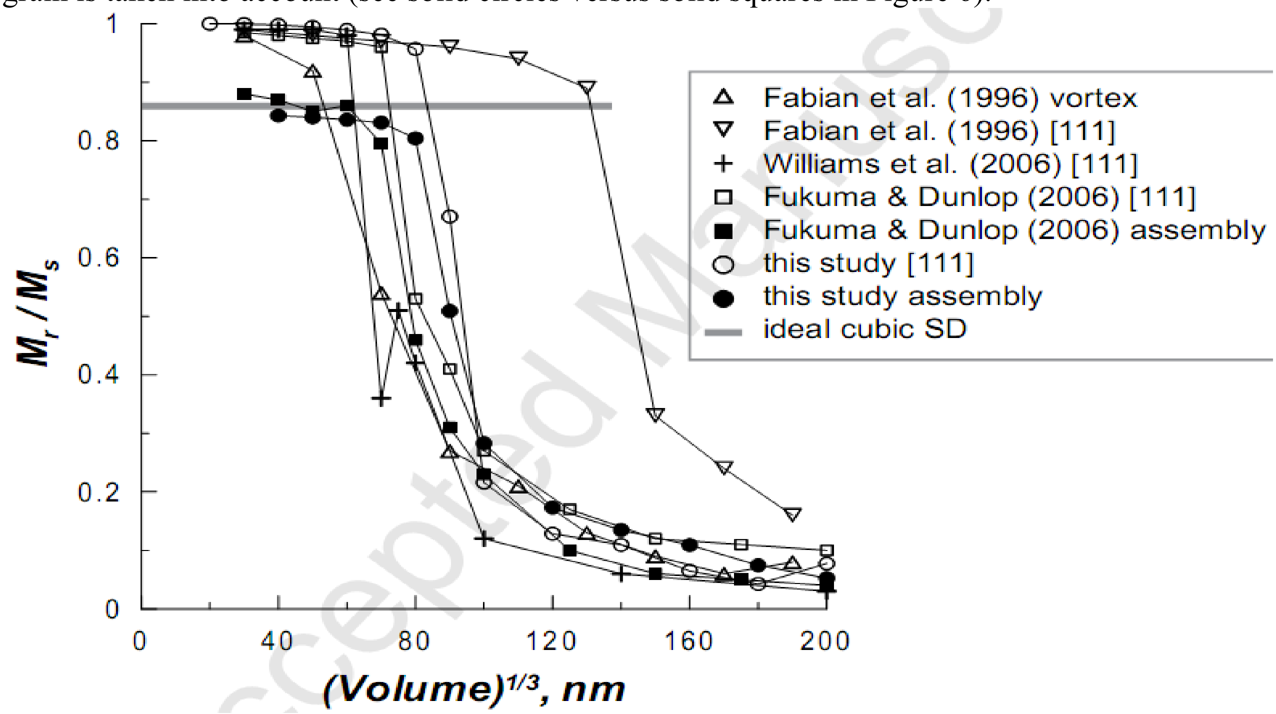

Discrepancy in estimated transition boundary of $Fe_3O_4$ may results from the difference in model code (a conjugate gradient method versus direct solution of Landau-Lifshitz-Gilbert equations.) and in element configuration (e.g., finite discrete model versus finite element model). In addition, difference in elemental size (i.e., exchange length) can also induce a difference in model solution. In the near future, it is strongly recommended that intensive inter-laboratory comparison with one another is required to check the consistency of the numerical solutions.

*4-2. Effect of Grain Elongation*

For the grains in SD-PSD transition size (~$10^6$ nm$^3$), the average coercivity and squareness values are plotted as a function of aspect ratio $q$ (Figure 7a, b).

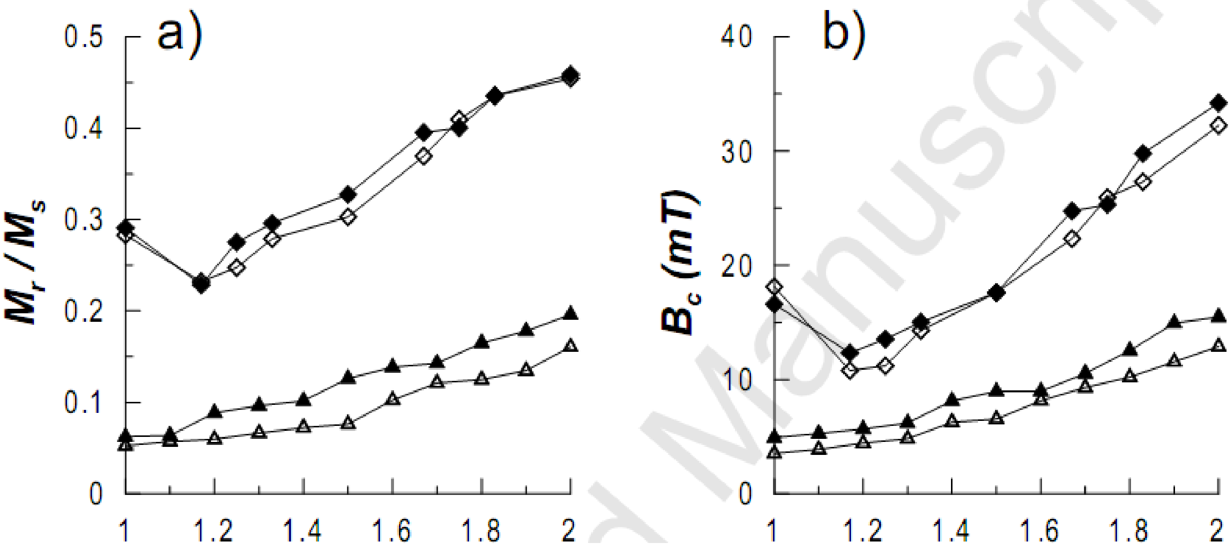


Both coercivity and squareness decreased as the aspect ratio increased from $q=1$ to $q=1.2$ due to a dominant magnetocrystalline anisotropy, but then they both increased as the aspect ratio increased further (Figure 7a, b). It is natural to observe the highest coercivity for $q=2$ due to a dominant magnetostatic-effect in elongated particles. In particular, values of squareness converged towards 0.5 as $q$ increased, mimicking a SD nature on a squareness-coercivity (SC) plot (Figure 7c). In this grain range, values of squareness and coercivity were virtually indistinguishable for both geometries (Figure 7a, b).

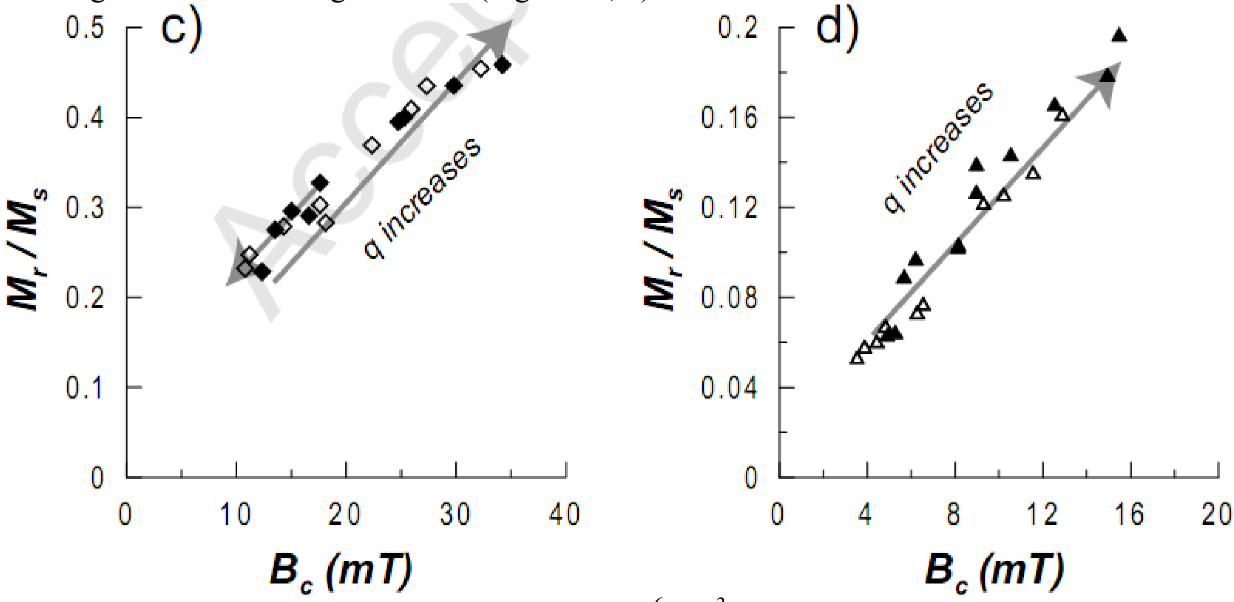


For the grains in much larger size (8 x $10^6$ nm$^3$), the coercivity and squareness were generally larger for octahedra (tetragonally terminated prism) than those for cubic (Figure 7a, b). As a result, hysteresis results for octahedral morphology were systematically biased towards the upper-right side in a SC plot than those for cubic geometry (Figure 7d).

*4-3. Morphology Dependence of Magnetic Hysteresis*

To check whether the grain morphology systematically produced larger coercivity and squareness for octahedral (tetragonally terminated prism) shapes, the average coercivity and squareness for $q$ =1.5 was plotted as a particle size of $Fe_3O_4$ (Figure 8). We used $q$ =1.5 as a standard because it is commonly observed as an average aspect ratio for many synthetic $Fe_3O_4$ grains (e.g., Levi and Merrill, 1978). Although the general trend appears to be similar, octahedra (and tetragonally terminated prisms) showed slightly higher coercivity and remanence ratio for > 120 nm than the cubes (and rectangular parallelepipeds) (Figure 8).

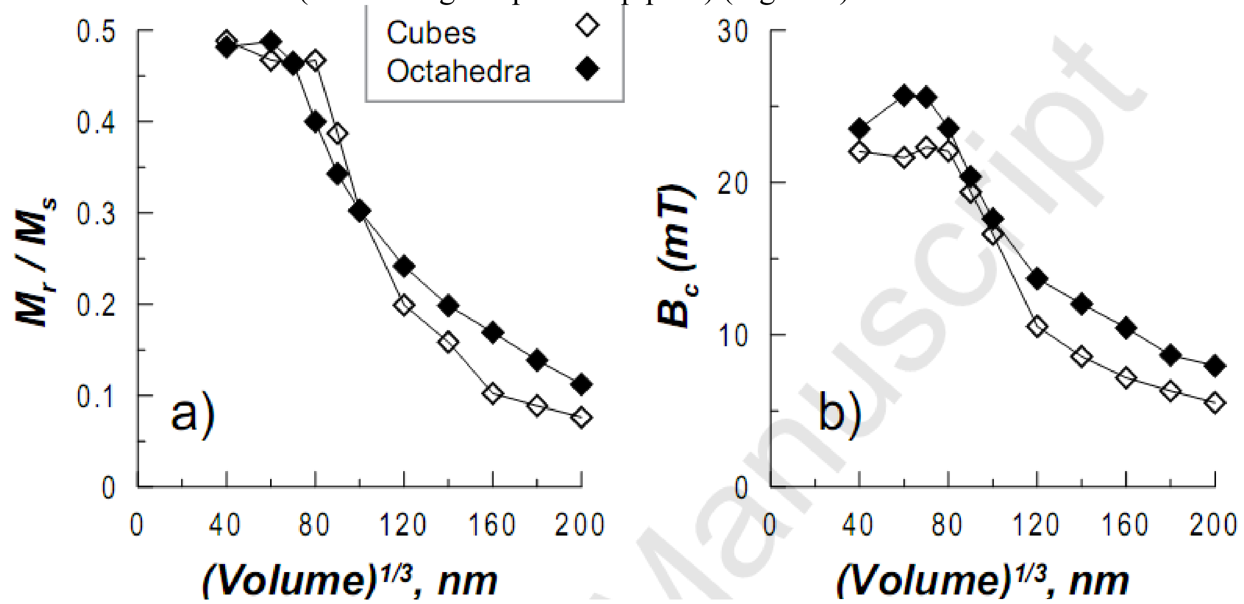


It is likely that octahedra are much more resistant to the variations of applied field resulting from an inherent geometric advantage (8 corners for rectangular parallelepipeds versus 10 corners for tetragonally terminated prisms), yielding slightly higher coercivities and remanences (Figure 8). More convincing evidence comes from a detailed microscopic configuration. In fact, simulations that yielded remanent magnetizations with vortex structures always showed higher coercivity for tetragonally terminated prisms than for rectangular parallelepipeds (Figure 3). In addition, forming a less efficient vortex state is another way to maintain a high squareness and coercivity for 200 nm of octahedra (Figure 4). Overall, particle size and grain geometry with detailed remanence configuration control the outcome of magnetic hysteresis properties.

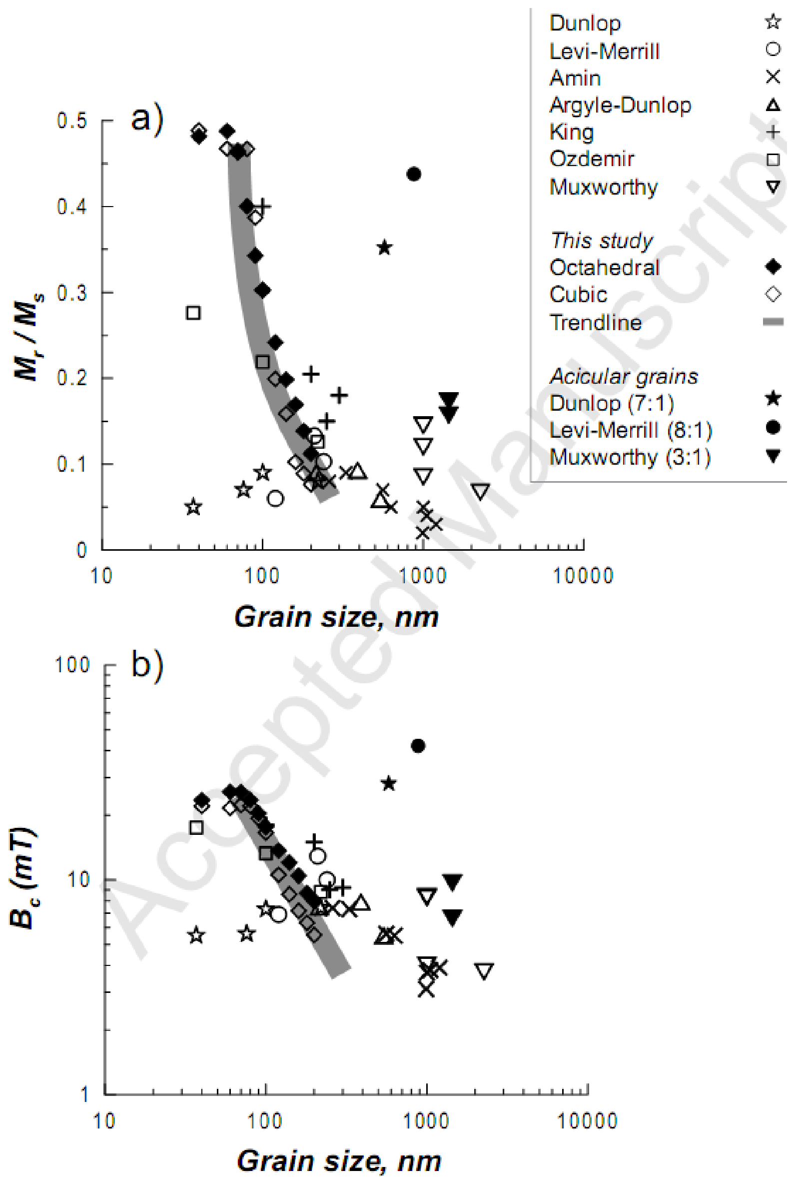


*4-4. Application to Published Data*

We compiled micromagnetic predictions with experimental measurements from the available representative data in the literature for stress-free $Fe_3O_4$ (Dunlop, 1973, 1986; Levi and Merrill, 1978; Amin et al., 1987; Argyle and Dunlop, 1990; King, 1996; King and

Williams, 2000; Özdemir et al., 2002; Muxworthy et al., 2006). From the wealth of data, we selected representative results whose grain size is less than ~2 μm (Figure 9). For clarity, we included only results whose coercivity is larger than 1 mT and squareness is larger than 0.01(Figure 9).

For stress-free $Fe_3O_4$, do our numerical simulation results (for both geometries) match roughly well with the previously reported dataset? With a few exceptions, the majority of experimental observations fell at upper-right side with respect to the simulation trend (Figure 9a, b). In particular, such systematic discrepancy between the simulation trend and the observed data is more distinctive for the coercivity data. Three potential sources of ambiguities may provide tentative solutions for such a systematic difference (Figure 9). First, it is likely that stress-free samples in the literature are not entirely stress-free. It is well-known that stress can substantially increase the magnetic coercivity and squareness. Second, as in other micromagnetic studies, we explored the effect of grain morphology with a constant volume condition. This approach makes sense in terms of physics because the magnetization is a function of grain volume. On the other hand, such constant volume approach would produce unanticipated ambiguity when converted as to represent the unit edge. It should be noted that the volume of equant octahedron with cube edge $a$ is $0.47a^3$. To be equivalent in volume, octahedron edge should be 29% larger than that for equant cubic. Such discrepancy is pivotal because almost all the experimental determinations of mean grain size of $Fe_3O_4$ in the rock magnetic literature used scanning electron microscope (SEM) images, where researchers obviously reported the major cube edge both for cubic and octahedron. Unless corrected (e.g., Yu et al., 2002), volume of octahedron morphology based on the SEM analysis would inherently be underestimated than that for cubic in practice. Third, SEM images cannot reflect the exact grain volume due to imperfect two-dimensional projection of three-dimensional objects (Kong et al., 2005).

There are three additional insights relating to magnetic hysteresis to be gained from outlier-results that fell far away from the majority of data (Figure 9). First, three acicular grains (Dunlop, 1973, 1986; Levi and Merrill, 1978; Muxworthy et al., 2006) displayed distinctively higher squareness and coercivities, indicating a prevalence of a uniaxial anisotropy. Second, effect of grain-interaction on magnetic hysteresis was recently investigated by Muxworthy et al. (2006). According to Muxworthy et al. (2006), both coercivities and squareness decreased as the degree of interaction increased (see three inverted open triangles at 1,000 nm) in Figure 9. It should be highlighted that interaction-high samples fell closest to other experimental data set, implying that non-lithographically produced $Fe_3O_4$ is probably influenced by grain-interaction to some extent. Third, values of coercivity and squareness for the fine-grained data (excluding the 240 nm one) of Dunlop (1973, 1986) are quite low, way too small to be sorely explained with stress and/or interactions (Figure 9). Perhaps, a wide grain size distribution with superparamagnetic contribution would produce such a unique behavior (see Fukuma and Dunlop (2006) for discussion).

## 5. Conclusion

Micromagnetic simulation for stress-free $Fe_3O_4$ showed a pronounced dependence on grain morphology and elongation. Octahedra (and tetragonally terminated prisms) showed higher coercivities and squareness for grain widths > 120 nm than the cubes (and rectangular parallelepiped). Given a dominant vortex state in this grain size range, an inherent geometric advantage makes octahedral more resistant to the variations of applied field. A compilation of micromagnetic calculations and experimental determinations for stress-free $Fe_3O_4$ illustrated slight mismatch, suggesting that stress-free $Fe_3O_4$ used in hysteresis experiments were not entirely stress-free or the grain size of stress-free $Fe_3O_4$ was overestimated on using two-dimensional images of three-dimensional objects.

**Acknowledgements**

This research was supported by NSF grant EAR0229498 to L. Tauxe and N. Bertram.

## References

Amin, N., S. Arajs, E. Matijevic, 1987. Magnetic properties of uniform spherical magnetic

particles prepared from ferrous hydroxide gels, Phys. Stat. Sol. A101, 233-238.
Argyle, K. S., D. J. Dunlop, 1990. Low-temperature and high-temperature hysteresis of small multidomain magnetites (215-540 nm), J. Geophys. Res. 95, 7069-7083.
Bertram, H. N., G. J. Zhu, 1992. Fundamental magnetization processes in thin-film recording media, Solid State Phys. 46, 271-371.
Carvallo, C., A. R. Muxworthy, D. J. Dunlop, 2006. First-order reversal curve (FORC) diagrams of magnetic mixtures: Micromagnetic models and measurements, Phys. Earth Planet. Inter. 154, 308-322.
Dunlop, D. J., 1973. Thermoremanent magnetization in submicroscopic magnetite, J. Geophys. Res. 78, 7602-7613.
Dunlop, D. J., K. S. Argyle, 1997. Thermoremanence, anhysteretic remanence and susceptibility of submicron magnetites: Nonlinear field dependence and variation with grain size, J.Geophys. Res. 102, 20,199-20,210.
Dunlop, D. J., 1986. Hysteresis properties of magnetite and their dependence of particle size: a test of pseudo-single-domain remanence models, J. Geophys. Res. 91, 9569-9584.
Fabian, K., A. Hubert, 1999. Shape-induced pseudo-single domain remanence, Geophys. J. Int. 138, 717-726.
Fabian, K., A. Kirchner, W. Williams, F. Heider, T. Leibl, A. Hubert, 1996. Three-dimensional micromagnetic calculations for magnetite using FFT, Geophys. J. Int. 124, 89-104.
Frankel, R. B., J-P. Zhang, D. A. Bazylinski, 1998. Single magnetic domains in magnetotactic bacteria, J. Geophys. Res. 103, 30,601-30,604.
Fukuma, K., D. J. Dunlop, 1997. Monte Carlo simulation of two dimensional domain structures in magnetite, J. Geophys. Res. 102, 5135-5143.
Fukuma, K., D. J. Dunlop, 1998. Grain size dependence of two-dimensional micromagnetic structures for pseudo-single-domain magnetite (0.2-2.5 μm), Geophys. J. Int. 134, 843-848.
Fukuma, K., D. J. Dunlop, 2006. Three-dimensional micromagnetic modeling of randomly oriented magnetite grains (0.03-0.3 μm), Geophys. J. Int. 134, 843-848.
Heider, F., D. J. Dunlop, N. Sugiura, 1987. Magnetic properties of hydrothermally re-crystallized magnetite crystals, Science 236, 1287-1290.
King, J. G., W. Williams, C. D. W. Wilkinson, S. McVitie, J. N. Chapman, 1996, Magnetic properties of magnetite arrays produced by the method of electron beam lithography, Geophys. Res. Lett. 23, 2847-2850.
King, J. G., W. Williams, 2000. Low-temperature magnetic properties of magnetite, J. Geophys. Res. 105, 16427-16436.
Kittel, C., 1949. Physical theory of ferromagnetic domains, Rev. Mod. Phys. 21, 541-583.
Kong, M., R. N. Bhattacharya, C. James, A. Basu, 2005. A statistical approach to estimate the 3D size distribution of spheres from 2D size distributions, Geol. Soc. Am. Bull. 117, 244-249.
Levi, S., R. T. Merrill, 1978. Properties of single-domain, pseudo-single-domain and multidomain magnetite, J. Geophys. Res. 83, 309-323.
Muxworthy, A. R., W. Williams, 1999a, Micromagnetic models of pseudo-single-domain grains of magnetite near the Verwey transition, J. Geophys. Res. 104, 29,203-29,217.
Muxworthy, A. R., W. Williams, 1999b, Micromagnetic calculation of hysteresis as a function of temperature in pseudo-single-domain magnetite, Geophys. Res. Lett. 26, 1065-1068.
Muxworthy, A. R., W. Williams, D. Virdee, 2003a, Effect of magnetostatic interactions on the hysteresis parameters of single-domain and pseudo-single-domain grains, J. Geophys. Res. 108, 2517, doi:2510.1029/2003JB002588.
Muxworthy, A. R., D. J. Dunlop, W. Williams, 2003b. High-temperature magnetic stability of small magnetite particles, J. Geophys. Res. 108, 2281, doi:2210.1029/2002JB002195.
Muxworthy, A. R., J. G. King, N. Odling, 2006. Magnetic hysteresis properties of interacting and noninteracting micron-sized magnetite produced by electron beam lithography, Geochem. Geophys. Geosys. 7(7), Q07009, doi:10.1029/2006GC001309.
Newell, A., D. J. Dunlop, W. Williams, 1993a. A two-dimensional micromagnetic model of magnetizations and fields in magnetite, J. Geophys. Res. 98, 19,393-19,403.
Newell, A., W. Williams, D. J. Dunlop, 1993b. A generalization of the demagnetizing tensor for

nonuniform magnetization, J. Geophys. Res. 98, 9551-9555.
Newell, A., R. Merrill, 1999. Single-domain critical sizes for coercivity and remanences, J. Geophys. Res. 104, 617-628.
Newell, A., R. Merrill, 2000. Size dependence of hysteresis properties of small pseudo-single domain grains, J. Geophys. Res. 105, 19,393-19,403.
Özdemir, Ö., D. J. Dunlop, B. M. Moskowitz, 2002. Changes in remanence, coercivity, and domain state at low temperature in magnetite, Earth Planet. Sci. Lett. 194, 343-358.
Rave, W., K. Fabian, A. Hubert, 1998. The magnetic states of small cubic magnetic particles withuniaxial anisotropy, J. Magn. Magn. Mater. 190, 332-348.
Schabes, M. E., H. N. Bertram, 1988. Magnetization processes in ferromagnetic cubes, J. Appl. Phys. 64, 1347-1357.
Seberino, C., H. N. Bertram, 2001. Concise, efficient three-dimensional fast multipole method for micromagnetics, IEEE Trans. Magn. 37, 1078-1086.
Tauxe, L., H. N. Bertram, C. Seberino, 2002. Physical interpretation of hysteresis loops: Micromagnetic modeling of fine particle magnetite, Geochem. Geophys. Geosys. 3(10), 1055, doi: 10.1029/2001GC000241.
Xu, S., D. J. Dunlop, Micromagnetic modeling of Bloch walls with Neel caps in magnetite, Geophys. Res. Lett. 23, 2819-2822.
Williams, W., D. J. Dunlop, 1989. Three-dimensional micromagnetic modeling of ferromagnetic domain structure, Nature 337, 634-637.
Williams, W., D. J. Dunlop, 1990. Some effects of grain shape and varying external magnetic fields on the magnetic structure of small grains of magnetite, Phys. Earth Planet. Inter. 65, 1-14.
Williams, W., D. J. Dunlop, 1995. Simulation of magnetic hysteresis in pseudo-single-domain grains of magnetite, J. Geophys. Res. 100(B3), 3859-3871.
Williams, W., T Wright, 1998. High-resolution micromagnetic models of fine grains of magnetite, J. Geophys. Res. 103, 30,537-30,550.
Williams, W., A. R. Muxworthy, G. A. Paterson, 2006. Configurational anisotropy in single-domain and pseudo-single-domain grains of magnetite, J. Geophys. Res. 111, B12S13, doi:10.1029/2006JB004556.
Winklehofer, W., K. Fabian, F. Heider, 1997. Magnetic blocking temperatures of magnetite calculated with a three-dimensional micromagnetic model, J. Geophys. Res. 102, 22,695-22,709.
Witt, A., K. Fabian, U. Bleil, 2005. Three-dimensional micromagnetic calculations for naturally shaped magnetite: Octahedra and magnetosomes, Earth Planet. Sci. Lett., 233, 311-324.
Yu, Y., L. Tauxe, 2005. On the use of magnetic transient hysteresis in paleomagnetism for granulometry, Geochem. Geophys. Geosys. 6(1), Q01H14, doi:10.1029/2004GC000839.
Yu, Y., D. J. Dunlop, Ö. Özdemir, 2002. Partial anhysteretic remanent magnetization in magnetite 1. Additivity, J. Geophys. Res. 107, 2244, doi: 10.1029/2001JB001249.
Yu, Y., D. J. Dunlop, Ö. Özdemir, 2003. Are ARM and TRM analogs? Thellier analysis of ARM and pseudo-Thellier analysis of TRM, Earth Planet. Sci. Lett. 205, 325-336.
Yu, Y., L. Tauxe, B. M. Moskowitz, 2004. Temperature dependence of magnetic hysteresis, Geochem. Geophys. Geosys. 5(6), Q06H11, doi:10.1029/2003GC000685.

**Figure Captions**

Figure 1. a) Partition of the particle with width *w*, length l, and cell size *s*. b) Schematic drawing for the arrays of octahedron (or tetragonally terminated prism). c) Relationship between applied field B and crystallographic axis. 9 is the angle of the easy axis of the grain with respect to the applied field B and *§* is the angle of the magnetization with respect to the easy axis.

Figure 2. Snapshots of magnetization configuration at the remanence state for *q=1.5,* 80 nm $Fe_3O_4$, B along [111]. Squareness was high (~0.4) for both geometries.

Figure 3. Snapshots of magnetization configuration at the remanence state for *q=1.25,* 140 nm $Fe_3O_4$, B along [100]. Both rectangular parallelepiped and tetragonally terminated prism show a vortex structure.

Figure 4. Snapshots of magnetization configuration at the remanence state for $q=1$, 200 nm $Fe_3O_4$, B along [001]. While both geometries show a vortex structure, octahedron $Fe_3O_4$ preserves squareness of 0.08, aligning magnetic spins along [001] for central 4 columns.

Figure 5. Variation of squareness (=saturation remanence $M_r$ / saturation magnetization $M_s$) as a function of aspect ratio $q$ (=major axis/minor axis) for 40 nm, 60 nm, 80nm, 90 nm, and 100nm $Fe_3O_4$.

Figure 6. Grain-size dependence of squareness for $Fe_3O_4$. For comparison, the results for other studies (Fabian et al., 1996; Fukuma and Dunlop, 2006; Williams et al., 2006) were also shown.

Figure 7. Variation of a) squareness (=saturation remanence $M_r$ / saturation magnetization $M_s$) and b) coercivity as a function of aspect ratio $q$ (=major axis/minor axis). Squareness-coercivity (SC) plot for c) 100 nm and d) 200 nm. Both coercivity and squareness decreased as the aspect ratio increased from $q=1$ to $q=1.2$ due to a dominant magnetocrystalline anisotropy, but then they both increased as the aspect ratio increased further.

Figure 8. Variation of squareness and coercivity of stress-free $Fe_3O_4$ ($q=1.5$) as a function of particle size. For > 120 nm, Octahedra (and tetragonally terminated prisms) showed higher coercivities and squareness than the cubes (and rectangular parallelepiped).

Figure 9. Compilation of micromagnetic predictions (this study) and experimental measurements from the available representative data in the literature for stress-free $Fe_3O_4$. Open and solid stars, Dunlop (1973, 1986); Open and solid circles, Levi and Merrill (1978); Ex, Amin et al. (1987); Open triangle, Argyle and Dunlop (1990); Cross, King et al. (1996) and King and Williams (2000); Open square, Özdemir et al. (2002); Open and solid inverted triangles, Muxworthy et al. (2006); Grey thick lines: trend line of micromagnetic simulation in this study.